

Influence of Interstitial Hydraulics on Plume Size and Shapes in Coastal Subsurface Foreshores

Okuroghoboye Diepreye Itugha, Emmanuel Munakurogha Adigio

Abstract— A non-invasive method called Visual Scaling Technique (VST) was applied to determine advective development of injected dye solution in estuarine beach-sand. It comprises site-survey, solute-injection, plume-recovery and data recording processes. Full 2-D plume-images of the contaminated area were captured using digital camera and details of the tail and topmost widths, plume vertical size, total travel height and subsidence depth measured. The geometric impressions of the plumes were found to vary with location detailing groundwater flow directions, hence contaminant pathways. The means of the plume development records in space was contrasted using time series, sequence and spectral plot models to find distinguishable periodic fluctuation components. It shows that groundwater and tidal water interstitial hydraulics influenced the shapes of the plumes. The time series and sequence plots show that no equal spacing and hint of seasonal variations were noticed except prominent fluctuations which identify with real time series. The spectral plots of the sizes and shapes of the plumes show upwardly varying daily growth of a time series but periodic fluctuation components could not be clearly distinguished. The spectral density appears to smoothen out the fluctuations arising from the non-periodic components of the data with the lowest frequency identified with the peak at 0.0417. The data therefore, confirm the existence of daily periodic components and that no other periodicities are identifiable. The model fits (seasonality and trend-cycle) in all cases fitted the observed data well, and it can be stated that both the seasonal adjusted series and trend-cycle models give the best exponential smoothing to the observed data.

Index Terms—Coastal foreshore, dye migration, plume size, interstitial hydraulics, groundwater table

I. INTRODUCTION

Tracer tests have been variously described in literature as invaluable tools for determining aquifer properties [1, 2]. The vadose zone (intermediary between seawater and groundwater) of the intertidal beach is affected by very complex hydrological processes from high-energy semidiurnal tides. The beach water table rises and falls with the sea level. So water-borne sewage or sewage discharged from urban, coastal recreational and industrial activities can enter and be retained or redistributed [3]. Other researchers [4] suggested that trace metals accumulated in beach sediments could be released by kinetic (advective) re-suspension processes and desorbed to the overlying watercourse. Accurate field studies/measurements are limited due to the complex hydrological environment as the

parameters controlling convective activity in-situ become more difficult to quantify [5, 6, 7]. As a result, there is presently poor understanding of the movement and spreading of anthropogenic substances (such as land-applied chemicals), spills and leaks that eventually enter beach sediments and consequently the freshwater domain (Maoet *al.*, 2006). This may partly explain that considerably more research is conducted on contaminant transport in coastal ground water (GW) aquifers than on transport in beach sediments [3, 8, 9, 10].

Pressure fluctuations can have a significant impact on interstitial oxygenation processes, thus on fates of contaminants and in some cases on aquatic life [7, 11]. Water movement is routed via complex pores and varies with depth and degree of compaction. The properties of the sand (porosity ϕ , grain size and grading) and the dye (density ρ , and dynamic viscosity μ) are therefore important to determine the role of hydraulic conductivity [12]. This is because the local unsaturated hydraulic conductivity depends on the degree of soil -water content and/or pressure head [13, 14]

In this study, fluctuation trends in the series of the plume size are mapped in seasonal adjusted series and trend-cycles, which reflect upward shift with the series values tending to increase over time. The upward trend is seemingly constant, which indicates a linear trend with dampening effects. The fluctuation patterns showing the daily account become clearer with increasing and relapsing peaks that characterize multiplicative and additive seasonality. The model fits (seasonality and trend-cycle) in all cases fitted the observed data well, and it can be stated that both the seasonal adjusted series and trend-cycle models give the best exponential smoothing to the observed data

II. EXPERIMENTAL DESIGN, MATERIAL AND METHOD

Site preparation, tracer type and dye injection have been extensively reported in Itugha et al. [18]. The design was such that each sampling point (SP) contains 3x5 or 5x5 injection points (IPs) over two rectangular arrays of 1.5 x 2.5 m² and 2.5 x 2.5 m² on the unsaturated beach surface. The rectangular arrays were divided into 0.5 (length, l) x 0.5 (breadth, b) m² square cells so that each SP consists of 15 or 25 injection points (IPs). Several initial tests on the field, informed the experiments to limit the solute volume injected per IP and depth to 5.0 ml and 0.05m respectively. Solute was injected into the natural sediments at the start of the low-tide water (unsaturation). The injected sample was monitored through several tidal cycles (1/4, 1, 2, 4, 6, 8, 10, 12, and 14) of winter (22/November 2005-19/January 2006) and summer (17/April 2006-17/July 2007).

Okuroghoboye Diepreye Itugha, Civil & Electrical/Electronic Engineering Department, Federal University Otuoke, 400 University Boulevard, Otuoke, PMB 126, Bayelsa State, Nigeria, Phone/ Mobile No. 00234 (0) 7033660771

Emmanuel Munakurogha Adigio, Mechanical/Marine Engineering Department, Niger Delta University, Wilberforce Island, Bayelsa State, Nigeria, Phone/ Mobile No. 00234 (0) 8064118064

The experiments were carried out at three OEIS injection zones (IZs), namely A, B, and C, and two NEIS injection zones, namely A and B. Each IZ defines multiple sampling points (SPs), which lists the total injected points and the mined injected points.) with two rectangular dimensions of $1.5 \times 2.5 \text{ m}^2$ and $2.5 \times 2.5 \text{ m}^2$ on the unsaturated beach surface. The rectangular arrays were divided into 0.5 (length, l) \times 0.5 (breadth, b) m^2 square cells so that each SP consists of 15 or 25 injection points (IPs) in 3×5 or 5×5 column/row grids (arrays) respectively [18]. In OEIS-IZ (A), out of the 855 total IPs at the 3×5 array 513 plumes were successfully mined. We will be considering OEIS-IZ (A) wells alone in this study because of the unique advective patterns of the plumes here.

A. Study Area

The experiments were conducted at the Outer Estuary injection site

(OEIS) and Narrows Estuary injection site (NEIS) of River Mersey Estuary (RME), New Brighton coast, $53^\circ 26' \text{N}$ and $003^\circ 02' \text{W}$ in Liverpool Bay (Figure 1). The Mersey Estuary of Northwest England has an area of approximately 5000 km^2 , which includes the major municipalities of Liverpool and Manchester, with a pollution history dating back to 1715 that made it one of the most polluted estuaries in Europe [15, 16, 17] Its catchment has a high density of population up to 5 million and heavily industrialized.



Figure 1: Area map with polygons showing the injection zones and Marine Lake at the sheltered boundary of the outer RME with overview maps (top-right inset shows the estuary and the catchment; the main map details the centre of the inset).

B. Tracer solution injection and monitoring

The dye solution (5.0ml portion) was injected at 0.05 m below the beach surface (about 1.55 m below the high tide mark) at the start of the low ebb-water. The choice of 0.05 m injection depth is considered to be reasonable since the first 0.05 m coastal sand region readily stimulates oxygen injection and utilization into deeper layers [19, 20]. A 10.0 ml Pressure-Lok precision sampling purge and trap syringe system with appropriately calibrated hypodermic needles of size $0.028'' \times 0.012'' \times 2''$ was used to inject the dye [18]. The injection always took place at the start of the low tide, therefore, there is no difference of start state of tide and the state of tide effect where the spread of dye is the same. Only the spectral results of the summer samples at OEIS-IZ (A and B) which are of a particular unique nature are reported here (Figure 1).

C. Tracer plume mining, measurement and parameterization

A 12-channel Garmin GPS 76 marine navigator (with precision of about $\pm 2 \text{ m}$) and Nikon Coolpix 8800 digital camera (with 8.0 effective megapixels) were used to identify/monitor IP locations and take 2D image photographs of excavated plumes. The injected dye was a red color 810 (E124) conservative agent with 4.3% pure dye content, and density of $0.947 \text{ g/cm}^3 - 1.022 \text{ g/cm}^3$. The contaminated surface area ($l \times b$) was detected and each boundary carefully sectioned using hand trowel to penetrate the undisturbed plume domain. The excavated plumes were so measured in the field (Figure 2). This means that the injected dye was entrapped within a volume of 0.13125 m^3 ($l=0.5$) \times ($b=0.5$) \times (depth $h=0.525$).



Figure 2: (a) about 4-5 hours after injection (no flood case), (b) after one complete tidal cycle and (c) two complete tidal cycles.

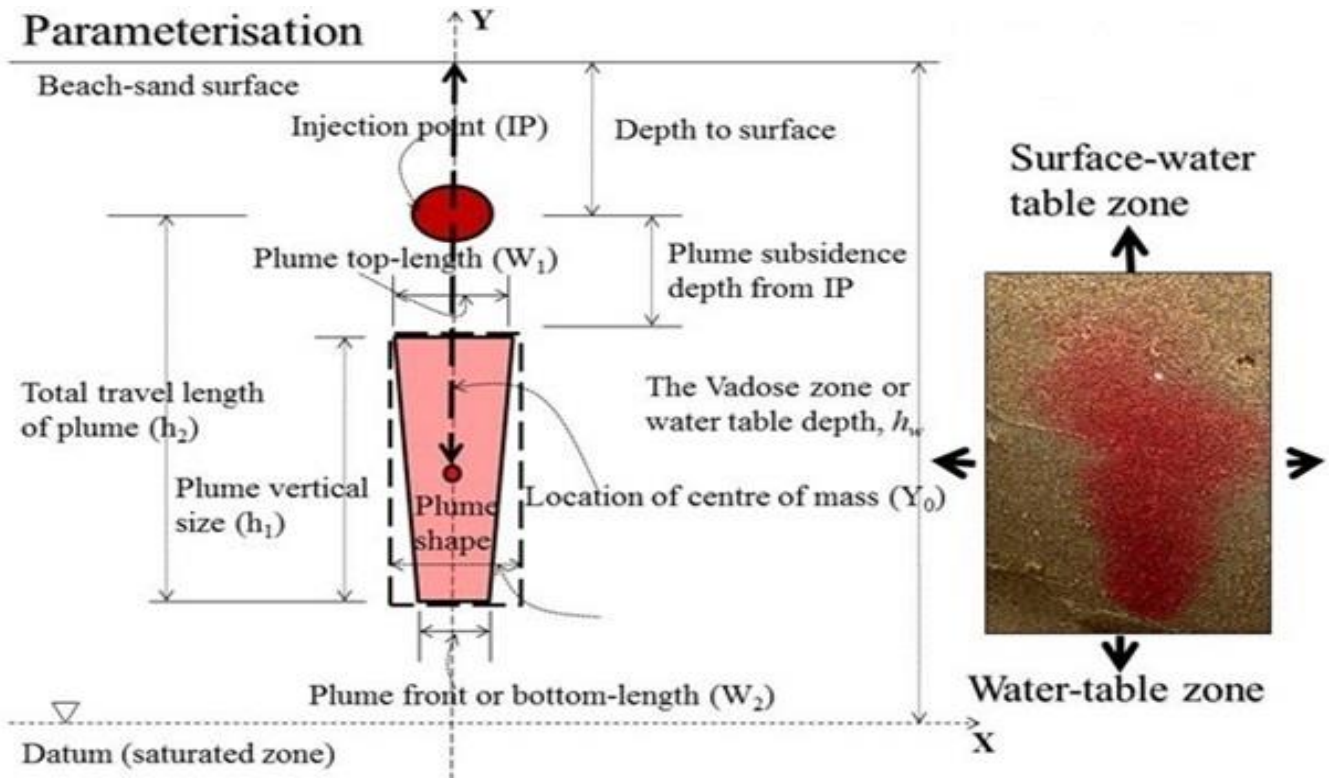


Figure 3: Depth-to-water and water-table elevation measurement

Figure 3 is the sketch to demonstrate and summarize these parameters where Cartesian coordinate system is established using the horizontal line passing the injection point as the x-axis and a vertical line some distance away from the plume center line as the y-axis. As the vertical advective spreading is a cone shape, a trapezoidal shape is adopted to evaluate the plume. The top and bottom (front) width of the plume is defined as W_1 and W_2 respectively. The infiltration depth is the vadose zone with horizontal infinite dimensions. The depth IP is the depth of injection ($IP = 0.05m$) while Y_0 represents the location of centre of mass, the depth of the center of mass of the cone (Y is the depth coordinate). Y describes the distance between the sand-surface water and sand-water table interfaces.

The foreshore is seaward-sloping (0.08389°) affected by semi-diurnal tides. The depth-to-water table (DTW) was taken as the depth below the beach surface to the top of the saturated material (subtidal), where the mean pore pressure is atmospheric [18]. The elevation and shape of the water table surface respond to surface water features resulted from recharge and discharge changes. The DTW measurements

averaged to about 0.525m, which is relevant towards understanding the depth of IP in relation to the high tide mark (HTM) [15]. The water-level data were converted from depth below surface to Water table elevation (WTE) using the GPS position at ground level, namely WTE was measured as the difference of beach surface elevation (BSE) and DTW

III. RESULTS AND DISCUSSIONS

The raw data of the plumes were processed using window based statistical software SPSS 15.1 and MS Excel. The objective of the process was to find the statistical significance of the dependence of the tidally induced pressure head on the assumed independent variables [total vertical displacement of plumes from ID ($Z = 0.05m$), horizontal displacement of the topmost plume widths (X_2) and tail (bottom) widths (X_1)]. **Table 1** of Day-1 to Day-5 shows the significance of the assumptions with details of least square expressions. The vertical dimensions for Day-1 here generally varied by $0.10758 \pm 0.00356m$ while the subsidence depth $0.09829 \pm 6.36E-3m$.

Table 1: Comparisons between results of least square model fit and measured VST field data

OEIS-IZ (A) Results										Collinearity Statistics	
TT-mean (hr)	X_1 (m)	X_2 (m)	Z_T (m)	Z_{plm} (m) (measured)	Z_{plm} (m) (predicted)	R-square (%)	F-ratio	P	Durbin-Watson Statistics	Tolerance	VIF
25.5371	0.03448	0.07177	0.15587	0.10758	0.09619	19.40	1.568	0.213	1.851	0.73-0.93	1.08-1.37
49.7023	0.03741	0.07614	0.23162	0.16203	0.14082	34.20	4.149	0.008	1.074	0.75-0.89	1.10-1.33
74.3596	0.03552	0.08006	0.29015	0.20197	0.18638	31.50	6.681	0.000	1.115	0.88-0.95	1.05-1.17
98.787	0.03989	0.08748	0.32736	0.20204	0.16147	33.50	2.775	0.052	1.437	0.67-0.97	1.02-1.49
125.81	0.05043	0.08286	0.33893	0.21464	0.25658	51.70	2.408	0.126	1.665	0.46-0.97	1.02-2.17

N/B: X_1, X_2 = initial and final plume widths respectively, VIF = variance inflation factor, TT = travel time, Z_{plm} = plume height = total plume travel height, plm = plume

The Durbin-Watson statistics value, 1.85, suggests that the residual errors show reasonable independence (Table 1). Also, the variance inflation factor (VIF) values (1.0-1.4) are well below 10 [19] and the tolerance level of the predictors falls between 0.73 and 0.93 which are well above 0.2 [20], making it safe to suggest that co-linearity is not a problem in this case. The variance proportions were also found to possess no multi co-linearity. Based on the co-linearity, Durbin-Watson and the F-ratio statistics, it will be reasonable to suggest that the effect of the model does not dent the substantive conclusion which shows significant validity in predicting the measured data. For instance the fitted linear regression model describes the variation in OEIS-IZ (A) plumes of Day-1 cycle have the form

$$Z_{plm} = 0.191(\pm 0.059) - 0.004(\pm 0.002)t + 0.049(\pm 0.130)Z_T + 0.420(\pm 0.519)x_1 - 0.206(\pm 0.188)x_2$$

The model was found consistent with the measured pressure head variables relative to the boundary conditions

Figure 4a shows that the velocity field for the low-tide is described by the gradient created due to the difference in the levels between the exit point and the over-height water level at low tide. However, the induced velocity causing this difference is higher compared to the velocity field due to the regional groundwater gradient. As the water level falls (Figure 4b) the infiltration water during the inundation of the unsaturated vadose zone is circulated outwards from the water table.

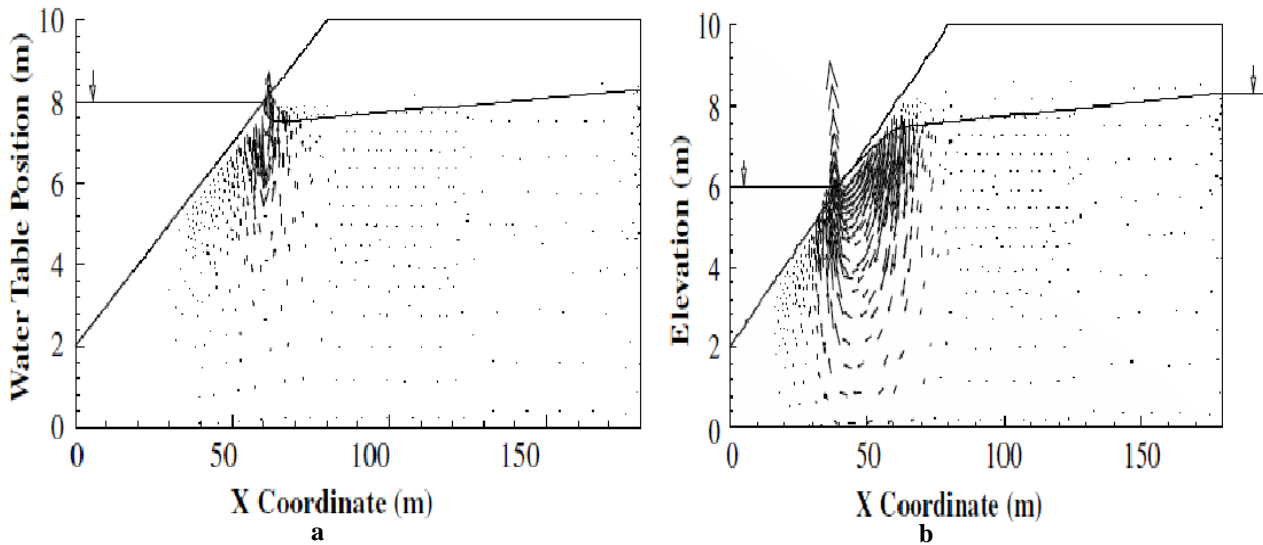


Fig 4: High and low water levels with velocity field distribution [24]

Figure 5a shows the time series plot while Figure 5b plot represents the box-plot of residual autocorrelation function using the means of Day-1 to Day-5 plume data for OEIS-IZ (A) from April and July. The time series plot describes the various time series models of measured parameters of the plumes with details of the observed and fitted estimates. The tail and topmost plume widths varied showing R^2 estimates of 0.13 and 0.25 with t-test values of about 27.32 and 25.7, while the plume-size and drawdown-length (subsidence from the surface) events had stationary R^2 values of 0.37 and 0.36 with t-test of 7.13 and 4.57, such that the probability of the t-test values occurring at zero intercepts in all the aforementioned parameters were less than 0.001 hence the effect of the predictor is significant and reflect a contribution in the development and dispersion of the solute plumes at the subsurface respectively. The root mean square error (RMSE) estimates for the tail & topmost widths, plume-size, and drawdown records 0.007, 0.017, 0.039 and 0.038 respectively. Also, the maximum absolute errors (MAE) and percentage errors (MAPE) for these parameters estimate to 0.006, 0.013, 0.029, 0.028 and 20.02, 21.08, 18.59, 41.51 respectively. The mean R^2 , RMSE, MAE and MAPE estimates for the time series model relative to the measured parameters as 0.327, 0.026, 0.20, and 18.78 respectively. Also, the tail & topmost widths were found to have additive

trends of plume variability, while the plume-size and drawdown differences show profiles of level shift and additive time series models.

The box-plot of residual autocorrelation function Figure 5b, varied on each model case with significant peaks for the tail and topmost widths at lags 2 UCL (upper confidence limits), 17 LCL (lower confidence limits) and lag 9 (LCL), 16 (UCL) respectively, while the plume-size peaked significantly at lag 2 (UCL) showing the non-seasonality function in the data. In addition, the data points of the residual ACF were well within the UCL and LCL of about $-0.25 < ACF < +0.25$. Also no statistical significance was observed in the Box-Ljung statistics.

The sequence plot in Figure 6 shows the time series of tail, topmost widths and plume-size respectively. The peaking patterns do not show equal spacing and no hint of seasonal variations but prominent fluctuations which are identical to real time series. Though the series possess some sense of seasonality individually by showing upwardly varying daily growth from the start of the summer months, the periodic fluctuation components cannot be clearly distinguished. While the tail and topmost widths may characterize additive patterns, the plume-size was seen to assume both multiplicative and additive trends.

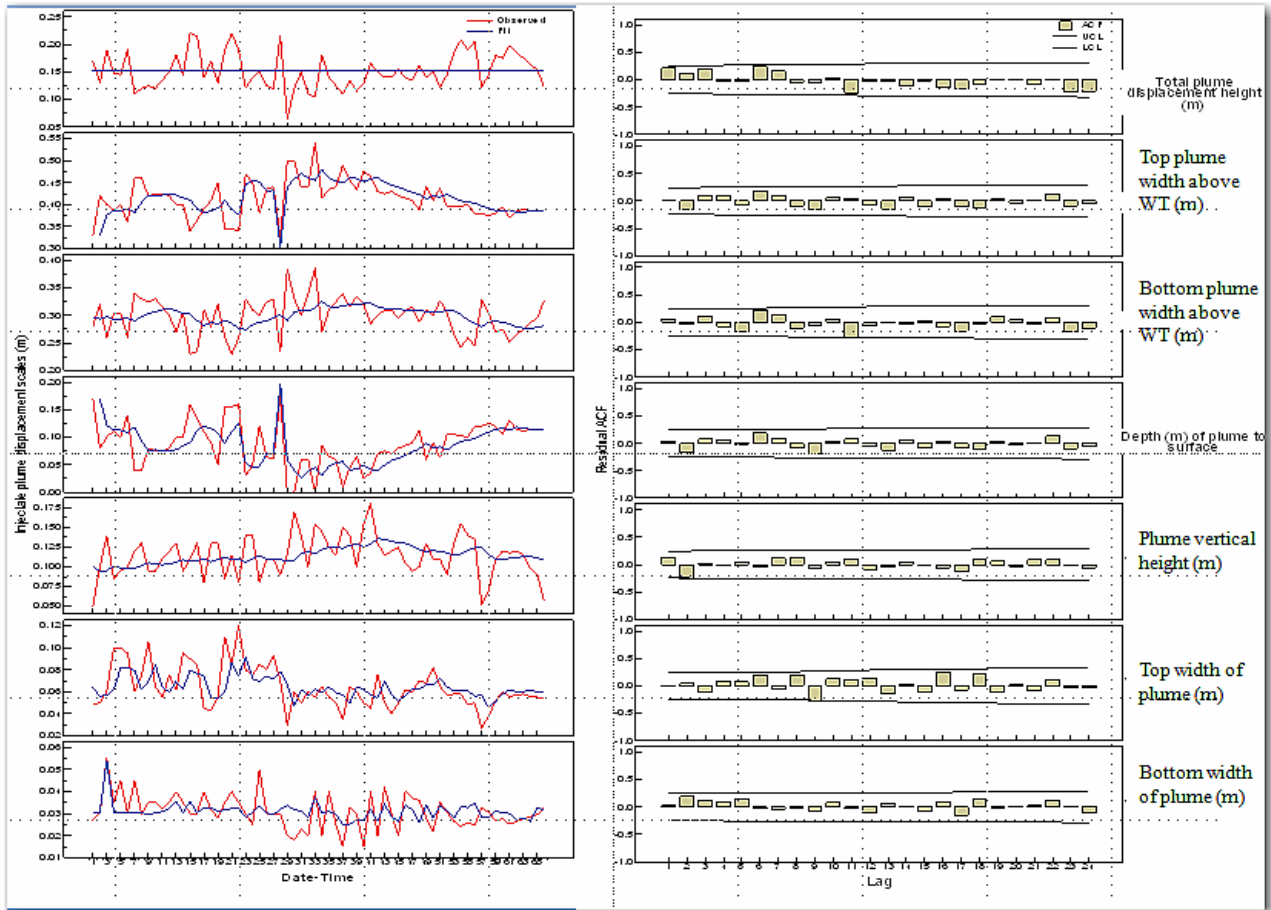


Fig 5: a. Time series models of injectate plume displacement scales showing observed and fitted curves; b. Box-plot of residual autocorrelation function for the measured injectate plume shapes.

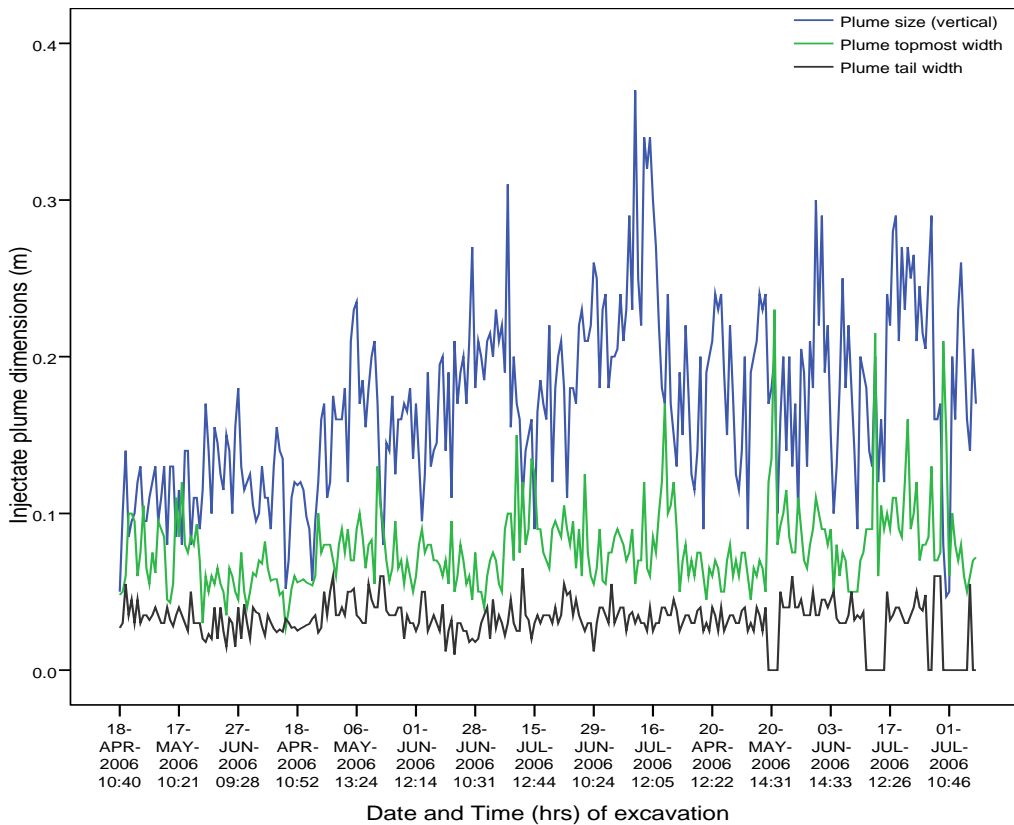


Figure 6: Time series plots of measured injectate plume events from Day-1 to Day-5 with varying fluctuations

The periodogram from the spectral plot shown in Figure 7 reflects sequence smoothing peaks that stand out from the background noise. The periodogram reduces with increasing frequency such that the lowest frequency peaks at a frequency of just about 0.03. That is, for frequencies of less than 0.1, the largest value in the Periodogram column occurs at a frequency of 0.03. We can categorise the contribution of the periodogram to a daily periodic component where each of the data points represents 24hrs (one day), that is to say a periodicity of 24hrs. This should result to a daily contribution peaking at about 0.0417, close to the 0.03 frequency where

the peak is established in Figure7. A further isolation of the background noise is carried out in Figure8 with a spectral density plot which appears to smoothen out the fluctuations arising from the non-periodic components of the data. The peaks deviated from sinusoidal behaviour but the lowest frequency identify with the smoothed version of the peak at 0.0417. The spacing of the peaks does not particularly show regularity in their trends, with series of varying higher frequency heights where the heights with the lowest peaks in the series occur at the frequency of the periodic component

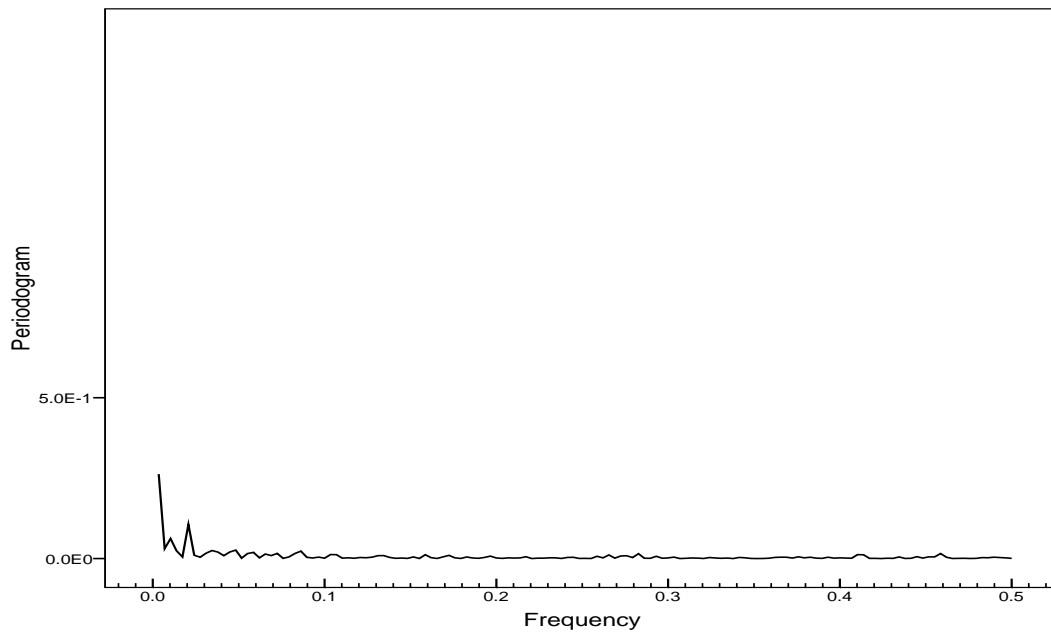


Figure 7: Spectral analysis of the injectate plume size (vertical) for the sequence (Day-1 to Day-5)

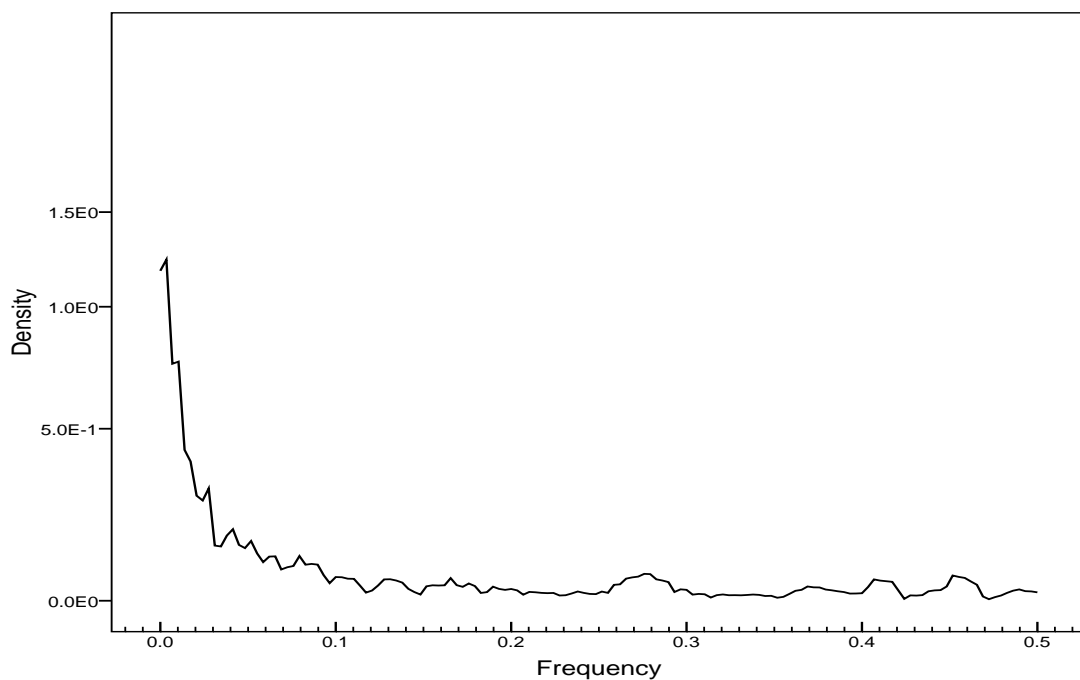


Fig 8: Spectral density analysis of the injectate plume size (vertical) for the sequence (Day-1 to Day-5)

The fluctuation trends in the series of the plume size are mapped in seasonal adjusted series and trend-cycles in Figure 9 and 10, which in both cases reflect upward shift with the series values tending to increase over time. The upward trend is seemingly constant, which indicates a linear trend with dampening effects from Day-3. The vertical reference lines partition the series into categories of highs such that the

fluctuation patterns showing the daily accounts become clearer with increasing and relapsing peaks that characterize multiplicative and additive seasonality. The model fits (seasonality and trend-cycle) in both cases fitted the observed data well, and it can be stated that both the seasonal adjusted series and trend-cycle models give the best exponential smoothing to the observed data.

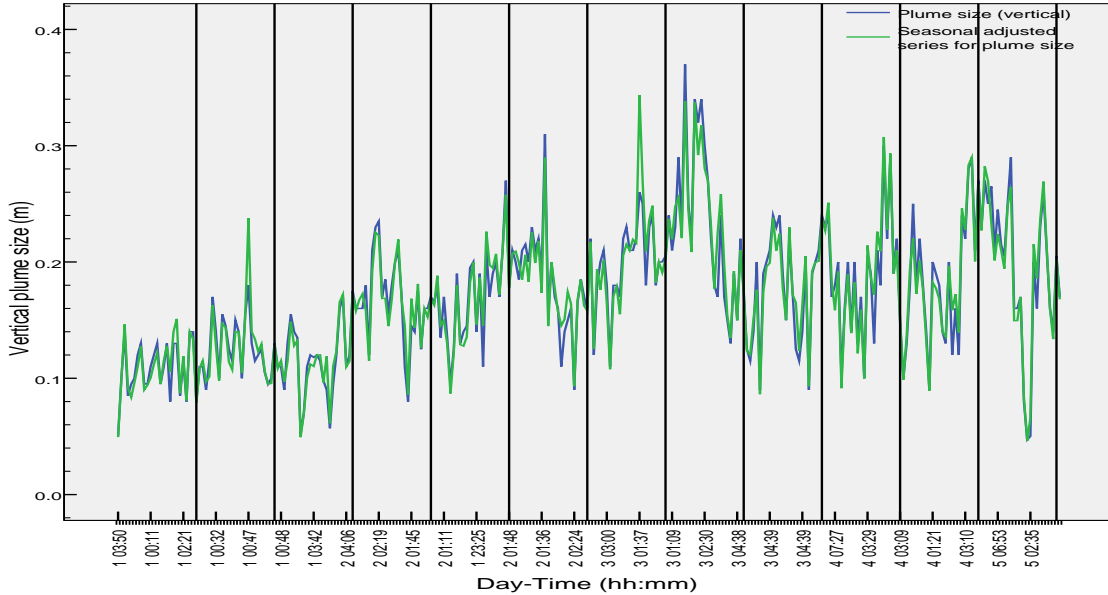


Fig 9: Sequence plots with observed and seasonal adjusted fits for the plume size (vertical) (Day-1 to Day-5)

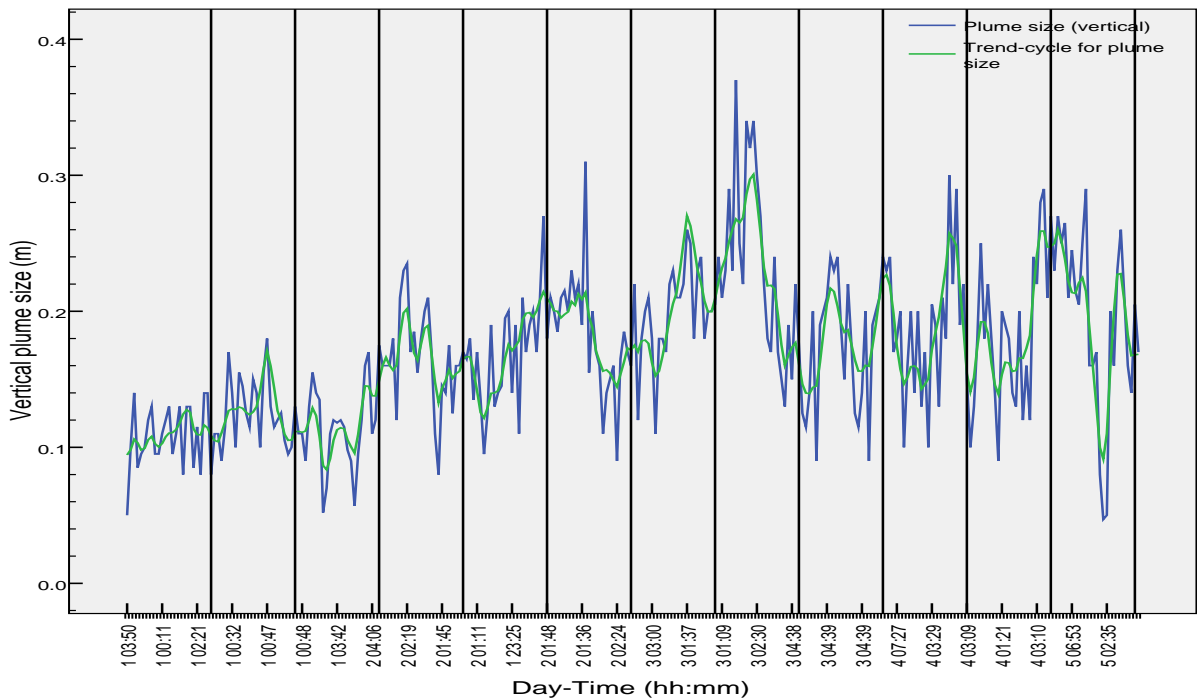


Fig 10: Sequence plots with observed and trend-cycle fits for the plume size (vertical) (Day-1 to Day-5)

IV. CONCLUSIONS

Plume maps at field scale from dye solute tests have been analyzed to show existence of transport function between the surface water and groundwater. This is significant because it shows how groundwater and tidal water interstitial hydraulics

influenced the shapes of the plumes. Partial regression plot with reference to tidal efficiency have shown sharp decline of the hydraulic fluctuations with increasing tidal efficiency. The linear correlation coefficient R^2 suggested 0.939 with the F-ratio of 1033.81 significant at $p=0.00$. The plume-size elevation fluctuations relatively decreased with time-lag with no periodicity.

In addition, the quantitative expressions of the plume data due to the transport function of the GWL as a consequence of the semidiurnal tides were used to create time series of plume sizes and shapes. Sequence plots were also created for the measured parameters respectively. No equal spacing and hint of seasonal variations were noticed except prominent fluctuations which identify with real time series.

However, the series possess individually upwardly varying daily growth from the start of the summer months, but periodic fluctuation components cannot be clearly distinguished. The tail and topmost widths characterise additive patterns while the vertical plume length (size) was seen to assume both multiplicative and additive trends.

The periodogram reduces with increasing frequency such that the lowest frequency peaks at a frequency of just about 0.03. We can categorise the contribution of the periodogram to a daily periodic component where each of the data points represents 24hrs (one day), that is to say a periodicity of 24hrs. This should result to a daily contribution peaking at about 0.0417, a close call to the 0.03 frequency where the peak was established. A further isolation of the background noise showed a spectral density plot that appears to smoothen out the fluctuations arising from the non-periodic components of the data with the lowest frequency identified with the peak at 0.0417.

The seasonal adjusted series and trend-cycles showed reflect of upward shift with the series values tending to increase over time. The upward trend is seemingly constant, which indicates a linear trend with dampening effects from Day-3. The vertical reference lines partition the series into categories of highs such that the fluctuation patterns showing the daily accounts become clearer with increasing and relapsing peaks that characterise multiplicative and additive seasonality. The model fits (seasonality and trend-cycle) in both cases fitted the observed data well, and it can be stated that both the seasonal adjusted series and trend-cycle models give the best exponential smoothing to the observed data.

REFERENCES

[1] J.M. Delleur, "The Handbook of Groundwater Engineering", CRC press LLC, Boca Raton, FL, 1999

[2] W. D. Weight, and J. L. Sonderegger, "Manual of Applied Field Hydrogeology, McGraw-Hill Companies, Inc., USA, 2001

[3] E.B. Diaw, F. Lehmann and P.H. Ackerer, One-Dimensional Simulation of Solute Transfer in Saturated and Unsaturated Porous Media Using the Discontinuous Finite Elements Method, *J. Contam. Hydrol.*, 2001, 51 (3e4), 197-213

[4] M. Martino, A. Turner, M. Nimmo and G.E. Millward, Re-Suspension, Reactivity and Recycling of Trace Metals in The Mersey Estuary, *UK. Mar. Chem.* 2002, 77 (2-3), 171-186.

[5] E. J. Wexler, Analytical Solutions for One-, Two-, and Three Dimensional Solute Transport In Ground Water Systems With Uniform Flow, USGS-TWRI Book 3, 1992, ChapB7

[6] Q.Zhang, R.E. Volker and D.A. Lockington, Experimental Investigation of Contaminant Transport in Coastal Ground Water, *Adv. Environ. Res.* 6, 2002, 229-237

[7] E. Precht, and M. Huettel, Rapid Wave-Driven Advective Pore Water Exchange in Apermable Coastal Sediment, *J. Sea Res.* 2004, 51, 93-107

[8] J.A. Lanyon, I.G. Eliot, and D.J. Clarke, Ground Water Level Variation During Semi-Diurnal Spring Tidal Cycles on a Sandy Beach, *Aust. J. Mar. Freshw. Res.* 1982, 33, 377-400

[9] X. Mao, P. Enot, D.A. Barry, L. Li, A. Binley and D. S. Jeng, Tidal Influence on Behaviour of a Coastal Aquifer Adjacent to a Low-Relief Estuary, *J. Hydrol.* 2006, 110-127

[10] M. Denham and K.M. Vangelas, Biogeochemical Gradients as a Framework for Understanding Waste-Site Evolution, Remediation, 2008, 19 (1), 5-17

[11] A. McLachlan, , *Water Filtration by Dissipative Beaches*, *Limnol.Oceanogr.*, 1989, 34(4), 774-780.

[12] C.W. Fetter, *Contaminant Hydrogeology*, Second ed. Prentice Hall Upper Saddle River, NJ, 1999, 7458

[13] R.K. Gupta, R.P. Rudra, W.T. Dickinson, and N.K. Patni, Wall, G.J., Comparison of Saturated Hydraulic Conductivity Measured by Various Field Methods, *Trans.*, 1993, ASAE 36, 51-55.

[14] B.P. Mohanty, M.D. Ankeny, R. Horton and R.S. Kanwar, Spatial Analysis of Hydraulic Conductivity Measured Using Disc Infiltrometer, *Water Resour. Res.* (inpress). 1994,

[15] WPRL, Effect of Polluting Discharges on the Mersey Estuary, Report of Investigations on Behalf of the Steering Committee on Pollution of the Mersey Estuary, WPRL Report 447R 1974

[16] P.D. Jones, The Mersey Estuary Back from the Dead: solving a 150-year old problem. *J. CIWEM*, 2000, 14, 124-130.

[17] C.H. Vane, I. Harrison and A.W. Kim, Polycyclic Aromatic Hydrocarbons (PAHs) and Polychlorinated Biphenyls (PCBs) in Sediments from the Mersey Estuary, *U.K. Sci. Total Environ.*, 2007, 374, 112-126.

[18] O. D. Itugha, D. Chen and Y.Guo, Pollutant Advective Spreading in Beach Sand Exposed to High-Energy Tides Estuarine, Coastal and Shelf Science 2016, 181, 70-82

[19] A. Rusch, M. Huettel and S. Forster, Particulate Organic Matter in Permeable marine Sands E Dynamics in Time and Depth, *Estuar.Coast. Shelf Sci.* 2000, 51, 399-414.

[20] S. Ehrenhauss and M. Huettel, Adjective Transport and Decomposition of Chain Forming Planktonic Diatoms in Permeable Sediments. *J. Sea Res.* 2004, 52, 179-197

[21] P. Nielsen, Aseervatham R, Fenton JD, Perrochet P. Groundwater Waves in Aquifers of Intermediate Depths. *Advances in Water Resources*, 1997, 20(1): 37-43.

[22] R.H. Myers, *Classical and Modern Regression with Applications*. PWS-Kent Publ. Co. Boston: Duxbury, 1990,

[23] S. Menard, *Applied Logistic Regression Analysis*, Thousand Oaks: Sage University paper series on quantitative applications in the social sciences, 1995, 7-106.

[24] B. Ataie-Ashtiani, R. E. Volker, and D. A. Lockington, Tidal Effects on Groundwater Dynamics in Unconfined Aquifers, *Hydrological Processes*, 2001, 15, 655-669